Towards the Complete Self-Sufficiency of a nZEBs microgrid by Photovoltaic Generators and Heat Pumps: Methods and Applications

Towards the Complete Self-Sufficiency of a nZEBs microgrid by Photovoltaic Generators and Heat Pumps: Methods and Applications

Filippo Spertino, *Senior Member, IEEE,* Alessandro Ciocia, *Member, IEEE,* Paolo Di Leo, *Member, IEEE,* Stefania Fichera, Gabriele Malgaroli, *Student Member, IEEE,* Alessandro Ratclif

***Abstract*— The present paper proposes a multidisciplinary procedure to correctly design a microgrid of all-electric nZEBs (nearly Zero Energy Buildings) from both electrical and thermal points of view. The procedure is suitable for new buildings supplied by local renewables, without the use of fossil fuel and with zero emissions. First, the thermal demand of each single nZEB is assessed, as a function of the installation site, building layout and physics, and material composing the envelope. Thanks to heat pumps, the thermal demand is transformed in electric load. Thus, the total electric consumption profiles, which include user's appliances and heating/cooling, are studied and compared with Photovoltaic (PV) generation supported by electrochemical storages. Both PV and batteries are simulated thanks to appropriate models. Regarding the PV production assessment, the present work proposes an improvement with respect to the use of traditional models, and it is based on experimental results on PV generators of recent production. The design methodology is applied to a real case of "energy community" composed of three nZEB units, that will be built in the campus of Politecnico di Torino, available to students and staff. The three units share PV production and storage capacity to reach the complete grid-independence.**

Keywords—nZEB, photovoltaic power systems, heat pumps, energy storage, thermal engineering, energy community, microgrid.

I. INTRODUCTION

The European Union is experiencing several challenges to increase energy efficiency and reduce polluting emissions. In the building sector, the main strategies consist of reducing the energy consumption and increasing local production from Renewable Energy Sources (RES), of which solar energy is generally the best solution for building integration. The result is the construction of nearly Zero Energy Buildings (nZEBs) with very high energy performance. In them the consumption must be significantly fulfilled by RES located on-site or nearby. The European Commission with the Directive 2010/31/EU outlines proper actions, at national level, in order to move the building sector in the direction of efficient and sustainable buildings. Starting from 2020, all new residential buildings will be nZEBs and the same requirement will be applied also to new buildings for commercial purposes from 2030 [1]. In this framework, universities will play a crucial role for the correct development of the nZEBs: innovative solutions, experimental results and guidelines will be provided. In many cases, researchers performed efficiency analysis resulting in retrofits actions in their university campuses [2][3]. In [4], authors analyzed several buildings in Soongstl University defining the best retrofit for each one and reaching an energy saving in the range 10—18%. In [5], through a real case study, different possible retrofits are studied with respect to energy savings and renovation costs for an existing school in Catalonia. Nevertheless, the energy efficiency in existing buildings is limited by the construction criteria used in the past. In several cases, it is not possible to reach the high performance of a nZEB. For this reason, the realization of new buildings is more interesting, because the energy and money savings are more profitable than the restructuring of old buildings. Some examples of these kinds of bindings are here reported. The Oberlin College Lewis Center (Ohio, USA) is a grid-connected Net Zero Energy Building (NZEB), that yearly produces equal or more electricity than it consumes. Nevertheless, the absence of storage determines a remarkable energy exchange with the electric grid. Furthermore, the CSIRO Energy Centre (Newcastle, Australia) is a nZEB combining RES, gas micro-turbine and storage system to simulate the integration of renewable sources in the grid. However, the building cannot be considered totally sustainable due to the use of traditional fuels for the gas turbine [6]. The Efficiency House Plus in Berlin is a residential housing module powered by Photovoltaic (PV) modules and equipped with a large battery storage. Its main issue is that the PV peak production is midday concentrated, while the residential demand is mostly in early morning and evening [7][8].

In the present work, a methodology to properly design nZEBs is presented, focusing on electrical and thermal aspects. The proposed procedure is dedicated to innovative buildings that do not consume fossil fuels and that are almost independent from the electricity grid, but exchanging power with the other nZEBs according to the new concept of energy community. To achieve this goal, the primary energy source will be mainly solar energy converted by PV generators (arrays of PV modules), supported by storage systems. They will supply the electrical consumption and the thermal demand of respective inhabitants, which use heat pumps for heating and cooling [9]. This methodology will be applied to design a new group of three nZEB units that will be built in the university campus of Politecnico di Torino. The building will consist of a single floor prefabricated wooden structure containing four adjoining rooms. The nZEB units will host students and staff and electronic equipment and the resulting load profiles are similar to that of tertiary sector buildings [10].

F. Spertino, A. Ciocia, P. Di Leo, S. Fichera, G. Malgaroli and A. Ratclif are with Dipartimento Energia "Galileo Ferraris", Politecnico di Torino, Corso Duca degli Abruzzi 24, 10129 Torino, Italy
(e-mail: { filippo.spertino, alessandro.ciocia, paolo.dileo, stefania.fichera, gabriele.malgaroli, alessandro.ratclif }@polito.it)

II. Proposed Methodology

The present work proposes a multidisciplinary methodology to correctly design totally electric nZEBs, with PV generation and heat pumps. The procedure requires electrical and thermal balances and can be applied to both tertiary sector and residential buildings. The procedure is described step by step in the following subsections.

A. Architectural design of nZEBs as "energy community"

The architectural approach, in the nZEBs under study, mainly deals with: first, the selection of appropriate 3D polyhedron shapes; second, the materials with minimum carbon footprint evaluated by the Life Cycle Assessment (LCA) method and, third, the ratio of the transparent to opaque surfaces.

Concerning the architectural geometry of the built environment, the typical polyhedra, starting from the simplest one, are the tetrahedron, the cube, the octahedron and so on. In this work, the chosen solid figures are, essentially, trapezoidal prisms in which the roof is not flat but sloped to host PV modules.

The embodied energy of materials for buildings is the main criterion to effectively choose the envelope in this procedure. Materials with low carbon footprint are stabilized mud blocks, terracotta tiles and wood. An example of structural wood is the glued laminated timber which will be used in this project and described in subsection III A. On the contrary, the use of glass for glazing is not favorable to keep a low carbon footprint and, thus, it is reasonable to prevail opacity with respect to transparency.

Therefore, the third aspect is strictly linked to the second because the building physics requires a low ratio of the transparent to opaque surfaces. In turn, the additional reason to adopt a ratio < 50% is to limit the thermal load in summer due to solar irradiance, and in winter the losses with respect to the internal heat generation. Moreover, such a low level of transparency guarantees a still acceptable natural lighting of the building and a proper separation between external and internal environment.

According to the concept of energy community, the main purpose is to reach the energy autonomy of the whole community. The economy of scale makes cost effective the investments in RES and the energy exchange is profitable for the members because it occurs at prices lower than those of the utility grid. The performance of the community is boosted thanks to the energy efficiency and load saving of nZEBs (with respect to traditional buildings). In this methodology, the users of the microgrid became an energy community. It means that in the design phase it is not anymore advisable to size the plants (i.e. PV and storage) for a single unit, but the whole community will be considered as a single user. Thus, all the generation plants will be sized to meet the consumption of all the users, and the share of production and storage will compensate for the possible poor matching between production and consumption for each single user.

B. Definition of thermal loads

The first step of the methodology consists of the determination of thermal loads. They are a function of the architectural layout and construction materials. The layout should guarantee an optimal use of available spaces as a compromise between a low thermal demand and an efficient exploitation of natural sunlight. Obviously, in many cases, there are constraints for the layout, the landscape and aesthetical requirements and urban planning [11]. The construction materials have to be structurally resistant with low polluting emissions. On the other hand, in order to minimize the thermal loads of the building, the materials have to guarantee a high thermal performance, minimizing the losses towards external environment. The energy balance between thermal gains and losses through the building envelope can be calculated for winter and summer. During winter, the building requires heat and the thermal demand $Q_{h,nd}$ is estimated according to equation (1):

$$Q_{h,nd} = (Q_{h,tr} + Q_{h,ve}) - \eta_{h,gn}(Q_{int} + Q_{sol}) \qquad (1)$$

The energy required by the heating system corresponds to the difference between transmission and ventilation losses ($Q_{h,tr}$ and $Q_{h,ve}$), and thermal gains Q_{int} and Q_{sol}. Transmission losses $Q_{h,tr}$ depend on several factors as the building envelope characteristics and the ambient conditions, according to the following equation:

$$Q_{h,tr} = H_{TR,glo} \cdot \Delta T \cdot \Delta t \qquad (2)$$

where $H_{TR,glo}$ is the heat transfer coefficient of the overall building envelope [W/K], ΔT is the difference between inside and outside temperature, and Δt is the time interval considered. In particular, $H_{TR,glo}$ depends on four contributions, according to UNI 13790 [12]:

$$H_{TR,glo} = H_{TR,D} + H_{TR,g} + H_{TR,U} + H_{TR,A} \qquad (3)$$

where $H_{TR,D}$ is the heat transfer coefficient towards external environments, while $H_{TR,g}$, $H_{TR,U}$ and $H_{TR,A}$ are the heat transfer coefficients towards the ground, non-air-conditioned rooms and adjacent buildings, respectively.

In general, each term H_x of equation (3) can be expressed as:

$$H_x = b \cdot \left[\sum(A_o \cdot U_o + A_{tr} \cdot U_{tr}) + \sum_k l_k \cdot \Psi_k + \sum_j \chi_j\right] \qquad (4)$$

where b is a correction factor equal to 1 if the considered envelope adjoins the external environment. In other cases (e.g. there are adjacent buildings), $b \neq 1$ and it is calculated according to [12]. The quantities A_o and U_o are, respectively, the surface and the thermal transmittance of opaque components of the envelope, while A_{tr} and U_{tr} refer to transparent surfaces. The influence of of the k^{th} linear thermal bridge is considered by the length l_k and the transmittance Ψ_k. Finally, for each punctual j^{th} thermal bridge, the thermal loss is calculated starting from the transmittance χ_j. The quantity $Q_{h,ve}$ in equation (1) indicates losses mainly due to air ventilation, that is required to maintain a high air quality. The ventilation losses are calculated according to the formula (5):

$$Q_{h,ve} = V \cdot n \cdot \rho_a \cdot c_a \cdot \Delta T \cdot \Delta t \qquad (5)$$

where V is the air volume in the room or building, n is the air changing rate per hour (1/h), ρ_a is the air density, c_a is the specific heat capacity of air. According to the Standard [13], typical values of n_{air} range between 10% and 20% of the air volume.

During winter, the thermal demands decrease due to the thermal gains. Q_{int} is the heat produced by internal sources such as human beings, electrical devices etc., and Q_{sol} is the energy coming from incident solar irradiance. However, only a part of these gains is actually useful to reduce the heating demand. Thus, the gains are multiplied by a reduction factor $\eta_{H,gn}$, defined in the Standard [12] between 0.7 and 0.8 for buildings with a good thermal behavior.

During summer, the thermal demand consists of cooling and it is estimated according to equation (6):

$$Q_{c,nd} = (Q_{int} + Q_{sol}) - \eta_{c,gn}(Q_{c,tr} + Q_{c,ve}) \qquad (6)$$

where $Q_{c,nd}$ is the thermal energy to be removed from the building. In summer configuration, Q_{int} and Q_{sol} are not gains, but additional contributions increasing the cooling demand. Concerning thermal gains, $Q_{c,tr}$ is the thermal energy exchanged with the environment due to transmission through the building envelope; while $Q_{c,ve}$ is the cooling gain due to air ventilation. The parameter $\eta_{c,gn}$ is the cooling gain reduction factor.

C. Definition of electrical loads

In order to maximize the use of local electrical RES, the thermal demand has to be converted into electrical demand. It can be easily performed by using electric and reversible heat pumps, which efficiently convert both heating and cooling demands in electrical loads [14]. Heat pumps basically use electricity to move heat from a cold space to a warm space. This is possible thanks to a mechanical-compression cycle refrigeration system that can be reversed to either heat or cool. This device is mainly composed of two heat exchangers (an evaporator and a condenser), a compressor and an expansion valve [15]. The efficiency of heat pumps in heating configuration is defined by the Seasonal Coefficient Of Performance (SCOP). This parameter is the ratio between the heating power output and the electric power input. In the same way, in cooling configuration, the Seasonal Energy Efficiency Ratio (SEER) is the ratio between the provided cooling power and the electric power input. Both SCOP and SEER depend on the difference between indoor and outdoor temperature [16]. According to [17], the average SCOP for commercial air-to-air heat pumps can be considered about 3.52.

In addition to the electric load of the heat pump, the other electric loads are the appliances in the building. In case of tertiary sector users, they consist of lights, computers and other electrical devices. Electric consumption profiles in offices has been already studied and they can be fairly predicted [18]. During winter holidays and nights of working days, a baseload is present for some electronic equipment, indispensable services and emergency systems. During working days, the consumption increases due to working activities. Consumption reaches the maximum value during morning (e.g. 09:00-13:00) and in the afternoon (e.g. 14:00-18:00), while a small drop occurs during lunch hour [19].

D. Design of optimal collection of solar energy

The production of a PV generator depends on the coordinates of the installation site and on the installation conditions, i.e. the azimuth and tilt of the modules. Obviously, to obtain the maximum production, modules have to be south-oriented in northern hemisphere, and the tilt shall be selected depending on the latitude. To this purpose, the PVGIS software provides a useful tool to define optimal tilt and azimuth for every site in Europe, Africa and Asia [20]. Starting from irradiance and temperature profiles, downloaded from PVGIS or other databases, or from weather stations, the production of PV generators can be estimated. It is possible to select the tilt useful to increase, as much as possible, the production during specific months (e.g. winter months, when radiation is minimum), or maximize the annual production. For example, Table I shows the variation of yearly in-plane radiation evaluated for four different orientations (South is the reference and West corresponds to $\gamma = 90°$) and for several tilt angles β between 5° and 70° with respect to the horizontal plane in Turin, Italy (latitude ≈ 45.07° N). In case of modules with better orientation ($-30° \leq \gamma \leq 30°$), the yearly optimal inclination is $\beta \approx 30°$ (first column).

TABLE I. YEARLY IN-PLANE VS TILT AND AZIMUTH ANGLES

β	**Yearly in-plane radiation (kWh/m²)**			
	γ=26°	**γ=-64°**	**γ=116°**	**γ=-154°**
10°	1510	1460	1340	1290
20°	1580	1490	1250	1150
30°	1620	1490	1160	1010
⋮				
70°	1410	1250	789	538

On the contrary, in case of poor orientations, modules shall be installed with lower inclination to maximize yearly solar collection. Another important aspect consists of the monthly distribution of energy production. If the goal is to increase the fulfillment of load during every season, the main issue is related to winter, when solar energy is low. As shown in Fig. 1, in case of a good orientation, a high tilt increases by more than 50% the winter collection, but worsens the summer collection. As a result, the yearly production is lower, but the monthly production profile is flatter. This solution can be used to better match constant loads during the whole year.

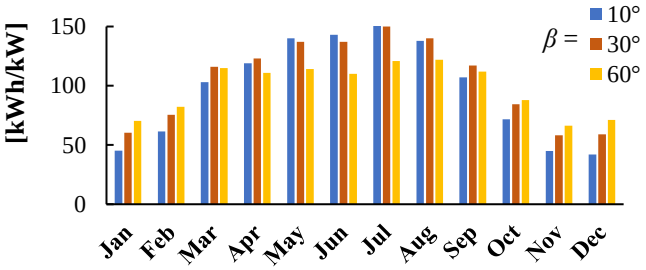

Fig. 1. PV production , with γ=26° (SW) and different inclinations β.

E. PV modelling

After the design of optimal collection for solar energy, the next step is the energy production of the PV generator from the irradiance and temperature profiles. In literature, the most used models is the Single Diode Model (SDM) with respect to the double diode model [21]. In the SDM, P_{DC} is calculated from the equivalent circuit which permits to trace the current-voltage (*I-V*) curve of a PV cell. Its relevant equation includes five parameters, with respect to the seven parameters of the double diode model [21], as follows:

$$I = I_{ph} - I_j - (V + R_s \cdot I)/R_{sh} =$$

$$= I_{ph} - I_0 \cdot \left(e^{\frac{q\cdot(V+R_S\cdot I)}{n\cdot k\cdot T_c}} - 1\right) - (V + R_s \cdot I)/R_{sh} \qquad (7)$$

where I_{ph} is the photo-generated current, I_0 is the saturation current, n is the quality factor of the junction, q is the electron charge, = $1.602\cdot10^{-19}$ C, k is the Boltzmann constant ($1.38\cdot10^{-23}$ J/K), R_{sh} is related to the insulation of the four lateral surfaces, R_s is the series resistance due to not ideal electrical contacts and T_c depends on irradiance G and ambient temperature [22]. The SDM can be represented according to electric circuit theory, as shown in Fig. 2.

The main issue for SDM consists of the correct definition of the 5 above-described parameters (I_{ph}, R_{sh}, R_s, n, I_0). Several sets of parameters are present in literature [23]; nevertheless, they are supposed constant values (i.e. they do not depend on environmental conditions, I_{ph} excluded) [24] or are related to old modules [25] or that can be used only for research purposes [26]. These data are not useful to correctly assess power and energy production of actual commercial PV modules. For this reason, in Section III, an experimental procedure is proposed for the calculation of the parameters. It permits the definition of their dependence on irradiance and temperature with commercial PV modules.

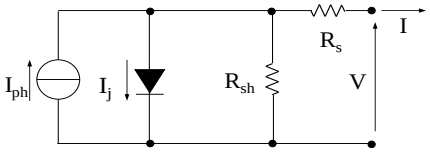

Fig. 2. Equivalent circuit of a PV cell based on the single diode model.

The DC power production P_{DC} is considered equal to the maximum value of the *P-V* curve. Then, AC production P_{PV} at T_c and G is calculated according to:

$$P_{PV}(G, T_c) = P_{DC}(G, T_c) \cdot \eta_{array} \cdot \eta_{PCU} \qquad (8)$$

The parameter η_{array} includes losses due to dirt, reflection from the glass, mismatch of *I-V* curves, and Joule effect in the cables. η_{PCU} takes into account the Maximum Power Point (MPP) tracking, DC/DC and DC/AC conversion [27].

F. Iterative PV sizing

The selection of the rated power of the PV plant is an iterative procedure and depends on the goal to achieve. If the requirement is the totally independence from the electric grid, the PV plant must supply the loads also in the worst condition. In particular, the sizing can start with a minimum PV size which guarantees an average daily production higher than the daily consumption during winter days. Then, if the results of the energy balance do not meet the load requirements, the size of the plant is increased, and the procedure is restarted. If the requirement is the total independence or nearly, at the end of the procedure the result could be an oversized plant for summer consumption, which could require a large surface, i.e. wide roofs and higher installation costs. Obviously, the sizing of the PV generator is correlated to the size of the storage, as written in the next sub-section.

G. Storage modelling and iterative sizing

Regarding the sizing of the batteries, the starting point for the definition of the minimum capacity is the average daily consumption during winter days; in other words, storage should supply all the loads at least for an entire day. The effectiveness of storage is related to the size of PV. If the PV generation is well sized and produces an average daily energy equal or higher than loads, batteries can store the midday surplus and discharge power during night hours. Obviously, a too big storage system is useless with an undersized generator, which production is already used by loads.

As in case of PV, the optimal size of storage is an iterative procedure: capacity should be increased, and calculation repeated, until the goal is reached. Nevertheless, in case of total independence from the grid, the system could require a high capacity, with consequent high costs [28].

The operation of batteries can be simulated thanks to the energy model [29]. This model does not require to measure physical quantities [30][31] and can be easily used to calculate the State Of Charge (*SOC*), i.e. the available energy capacity of the batteries, at any time instant t_i. In case of batteries discharge, the formula to be used is (9), while (10) defines the charge:

$$SOC(t_i) = SOC(t_{i-1}) - \frac{P_{bat}(t_i)\cdot\Delta t}{C_{E,bat}} \qquad P_{bat} > 0 \quad (9)$$

$$SOC(t_i) = SOC(t_{i-1}) - \frac{\eta_{bat}\cdot P_{bat}(t_i)\cdot\Delta t}{C_{E,bat}} \qquad P_{bat} < 0 \quad (10)$$

$SOC(t_{i-1})$ is the state of charge of the storage at the previous time instant t_{i-1}, P_{bat} is the exchange between the batteries and the system in terms of average power in the time step Δt, η_{bat} is the efficiency of the storage in charging operation and $C_{E,bat}$ is its capacity in kWh. Batteries are generators in discharge ($P_{bat}>0$), providing energy to the loads, while in charging operation ($P_{bat}<0$), the storage units absorb energy from PV generators, behaving like loads. However, the behavior of the storage is not ideal, and several factors can influence its performance, leading to batteries aging. In particular, not optimal charging patterns, overcharging, undercharging and abnormal cycling conditions, caused by atypical charging temperature, can degrade the batteries. Generally, two limits are imposed on storage units to protect them from aging: in particular, a power limit ($P_{bat}<P_{bat,max}$) avoids too high currents to circulate in the units, while an energy limit ($SOC \geq SOC_{min}$) avoids the complete discharge of the batteries. In addition, the full capacity cannot be exceeded ($SOC \leq SOC_{max}$). Typical energy limits for lithium batteries are in the ranges SOC_{min}=0.05—0.2 and SOC_{max}=0.9—1, while for lead acid batteries SOC_{min} is 0.5. Regarding the power limit, it varies greatly depending of technical data of the storage [32].

H. Power balance and self-sufficiency calculation

The main goal of a nZEB is to reduce the energy supply from external sources. In case of an all-electric nZEB, it means that PV and other electric RES have to meet, as much as possible, the loads to minimize the electricity absorption from the grid. According to equation (11), the power exchanged with the grid P_{grid} at each time instant t_i can be calculated as the balance between the consumption P_{load}, the PV production P_{PV} and storage P_{bat}, where the generator sign convention is used:

$$P_{grid}(t_i) = P_{load}(t_i) - P_{PV}(t_i) - P_{bat}(t_i) \qquad (11)$$

To quantify and compare the performance of the nZEB, the self-sufficiency amount R_{ssuff} is calculated. It can be calculated for any time interval, and it is the ratio between the loads locally supplied by RES and storage E_{lgc}, and the total load E_{load} [33]:

$$R_{ssuff} = E_{lgc}/E_{load} \qquad (12)$$

The energy E_{lgc} includes the contribution of the PV energy locally generated and immediately consumed, and of the energy provided by the storage; therefore, the presence of batteries is fundamental to increase R_{ssuff}. The self-sufficiency is different from the self-consumption; in fact, as described in [34], the self-consumption is the ratio between the energy immediately consumed and the production $R_{scons} = E_{lgc}/E_{PV}$.

For example, Fig. 3 shows PV generation and consumption profiles of tertiary sector users during a winter day. In the morning, the batteries are fully charged and they can supply the loads until 11:00 a.m. (E_{dis} is the storage discharge). After 11:00 a.m., load is lower than PV production, and storage is charged (E_{ch} is the storage charge). This amount of energy is used later, from 14:30 to 17:00, when PV generation is not sufficient for the electrical demand. Later, storage is empty and the loads are totally supplied by the grid (E_{abs}). As shown in the graph, E_{load} corresponds to the sum of the energy immediately produced and used E_{lgc}, the energy discharged from batteries E_{ch}, and the energy absorbed from the grid E_{abs}.

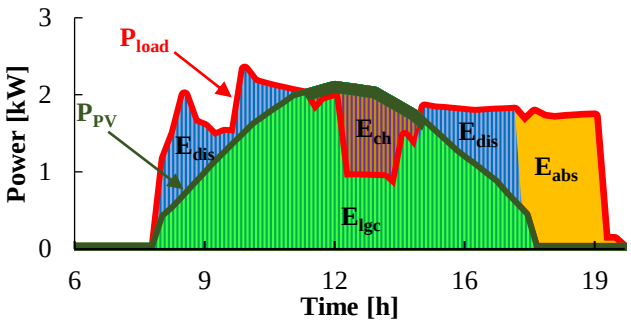

Fig. 3. Example of PV production, storage and load profiles.

The last step of the procedure consists of the check of the level of self-sufficiency reached with the selected configuration. If it satisfies the requirements, the procedure is complete. Otherwise, improvements are possible acting on the parameters influencing the performance. First, the sizes of RES and storage can be changed, and the simulation procedure repeated until the correct sizes are reached. Nevertheless, in some cases there are constraints in terms of maximum PV size and storage capacity, such as limited spaces, or a low budget. Then, if the plants cannot be upgraded, the load must be reduced. Regarding thermal load, it can be reduced by furtherly increasing the isolation of the building, or changing its architectural characteristics. Regarding electrical loads, a Demand Side Management (DSM) can be performed to better locally match the electric production from PV. Buildings have significant number of flexible loads [35]. Therefore, the DSM can be useful especially considering the presence of manageable devices as the heating, ventilation and air conditioning systems, by shifting loads in time and using the thermal inertia of the building [36]. The last possible solution is load shedding, i.e. the reduction or interruption of not essential loads. It can be adopted anticipating the closing hour of the building; e.g., when PV is low and storage empty in the worst winter days. After the load reduction or the DSM, the above described iterative procedure is repeated to evaluate the new performance of the system. Fig. 4 shows a flowchart containing the above described steps composing the iterative procedure.

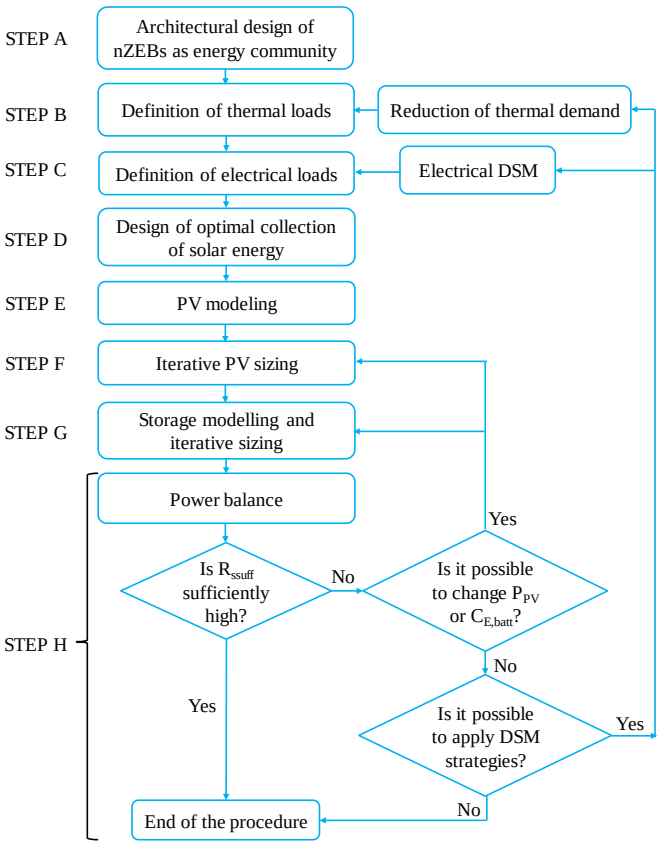

Fig. 4. Proposed methodology for the design and simulation of nZEBs.

III. Application of the Methodology to an Innovative All-Electric nZEBs Microgrid

Section II defines a procedure to correctly design a single nZEB, from both thermal and electric point of views. In the present Section, this procedure is applied for the design of a microgrid, where all the buildings (or units) will be nZEBs. The microgrid will be built in the campus of Politecnico di Torino and it will include 3 units, working as independent systems: the first unit (unit #1) will contain a technical and a control room, while the other two units (unit #2 and unit #3) will be study rooms.

A. Architectural design of nZEBs as "energy community"

The nZEBs will be built in the university campus of Politecnico di Torino offering tertiary sector services. They will operate as a microgrid representing an energy community. The microgrid will consist of four buildings (trapezoidal prisms) corresponding to three autonomous housing modules or units with different entrances, and independent thermal and electric plants. The sloping roofs of the nZEBs will host PV modules to meet the consumption of the units.

The total floor surface of all the units will be 105 m^2 and the inner volume 315 m^3. In the study rooms, students and staff will study and work, while in the control room a continuous monitoring of the system will be carried out. The technical room will contain the energy conversion devices and the storage units.

In Fig. 5, the layout of the nZEB is presented for 21st December at 15:30.

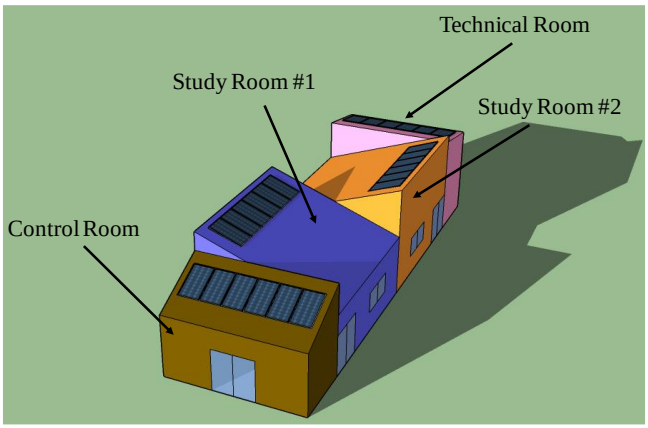

Fig. 5. Layout of the nZEB on 21st December at 15:30

The three units will be built with an eco-friendly material. The Glued Laminated Timber (GLULAM) consists of multiple layers of solid wood lumber bonded together with high-strength adhesive to form a single structural unit. This material is selected for its structural and thermal characteristics. Its flexibility guarantees high resistance even in case of earthquakes [37], thus GLULAM can be used to build the supporting structure. In addition, the net life-cycle emission is zero, and it has low thermal conductivity. Finally, wood guarantees the thermal comfort: it absorbs the humidity when it exceeds the saturation level and it releases vapor when humidity is too low. Regarding the ratio of the transparent to opaque surfaces, in this project, it is ≈ 21% to guarantee an optimal compromise between the building physics and the architectural requirements.

The block diagram of the microgrid is shown in Fig. 6. In each unit composing the microgrid, a device, including a Maximum Power Point Tracking (MPPT) and a Battery Management System (BMS), is connected to PV generator and storage system, respectively. The MPPT must continuously extract the maximum power from PV in any environmental conditions [38][39], while the BMS controls storage charge and discharge to guarantee the correct operation of batteries. A single unidirectional DC/AC converter permits to supply the local AC loads. The Microgrid Management System (MMS) is the core of the microgrid. It consists of a device which manages the loads according to the production of PV systems and the *SOC* of battery units. The MMS continuously communicates with the BMSs (dashed green lines) and the converters of all the units to decide how to connect loads according to the procedure described below. Breakers inside the MMS are used to disconnect the loads from their unit and connect them to the other units or the grid. The electronic equipment inside the MMS permits a practically interruptible supply of loads, also during the switching between the units or the grid. An example of the application of the above described logic is present in subsection III H.

The conversion efficiency η_{PCU} is considered 97% and the other generation efficiency is η_{array}=92%. Regarding storage, a charging efficiency η_{bat}=96% is used.

An appropriate measurement system will be used to monitor all the power profiles in each unit and the efficiency of devices (e.g. PV power productions, storage charges and discharges, DC/AC and DC/DC conversion efficiencies, energy exchanges between units, absorptions and injections into the grid).

The primary aim of the system is the almost complete independency from the electricity grid, with loads mainly satisfied by PV. For this reason, unidirectional converters do not permit the charge of the storage from the grid. The use of a single unit for both PV and storage avoids an additional conversion stage (with respect to a storage connected to the AC side), increasing the overall efficiency of the system.

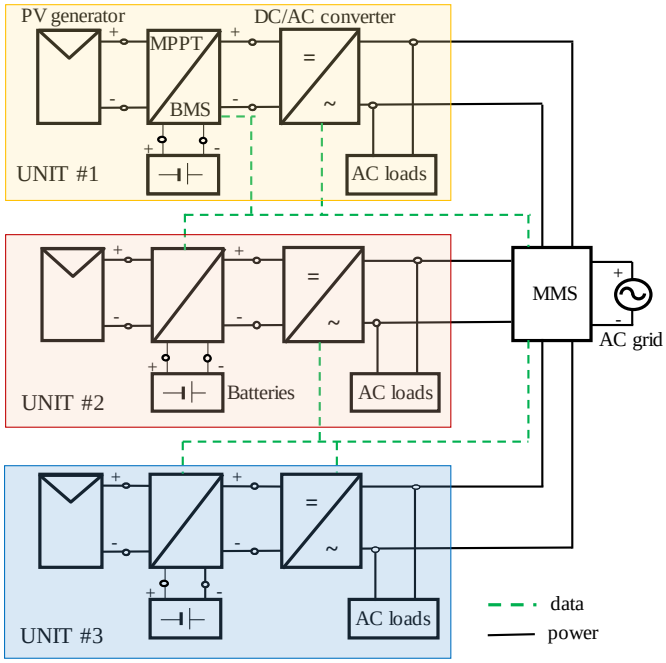

Fig. 6. Electric scheme of each unit of the microgrid.

Regarding the management of the microgrid, the self-sufficiency is maximized at the level of the whole energy community. Thus, each unit firstly has to satisfy its own loads, then it is helped by the neighbors, and the use of the grid is always the last chance. The procedure works as follows:

- First, loads of each unit are supplied by respective PV arrays and batteries. In case of surplus, the local storage is charged.
- After the fulfillment of local loads and battery charge, in case of an additional surplus, each unit exchanges power with the other units thanks to the MMS. In particular, the MMS connects the loads of the units in deficit to the units with surplus or available stored energy.
- Finally, if the surplus or storage of one or more units cannot supply the others in deficit, the units in deficit are connected to the grid. On the other hand, if the surplus of a unit cannot be absorbed by low loads of the other units, it is injected into the grid.

B. Determination of thermal loads

In the present work, the heat transfer coefficients $H_{TR,A}$ and $H_{TR,U}$ (described in subsection II B) are zero and the parameter b = 1, because there are no adjacent buildings or unconditioned rooms. Moreover, $H_{TR,D} >> H_{TR,g}$ and thermal bridges are negligible, therefore it is assumed:

$$H_{TR,glo} \cong H_{TR,D} \cong \sum(A_o \cdot U_o + A_{tr} \cdot U_{tr}) \qquad (13)$$

Representative values of thermal transmittance, for non-residential buildings in Italy, range between ≈ 0.78 W/m^{2}K and ≈ 1.95 W/m^{2}K for opaque components. On the contrary, they vary between ≈ 2.80 W/m^{2}K and ≈ 5.65 W/m^{2}K for transparent surfaces [40]. Regarding the annual energy consumption, the most efficient Italian houses satisfy the class A requirements: in particular, according to [41], transmittance values of class A buildings have to be U_o < 0.26 W/m^{2}K in case of opaque components and U_{tr} < 1.40 W/m^{2}K for transparent surfaces. In order to obtain even higher performance, the present living module is designed to have average transmittance values U_o = 0.15 W/m^{2}K and U_{tr} = 0.78 W/m^{2}K for opaque and transparent components, respectively. These parameters permit to obtain the Passive House Institute certification [42] (specific energy consumption due to seasonal heating < 15 kWh/(m^{2}y)). To obtain these results, the overall thickness of walls is more than 30 cm; in case of windows, the thickness of glasses is more than 3 cm. The stratigraphy of the opaque and transparent envelope of the nZEB is presented in Fig. 7, with the thickness of each layer δ:

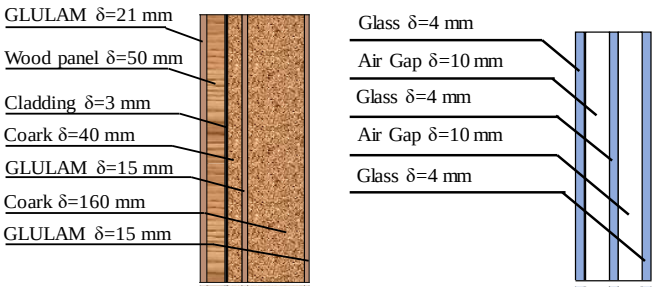

Fig. 7. Stratigraphy of the opaque (left) and transparent (right) nZEB envelope

Each unit, compositing the nZEB, has a separate air-to-air heat pump to satisfy heating and cooling demands. Each heat pump has a rated electric power of 2 kW, with an efficiency SCOP= 3.5. The ventilation systems guarantee an appropriate level of comfort, with a ventilation rate n_{air}=15% for each unit. Regarding thermal yearly demands, the whole nZEB requires 1509 kWh for cooling and 1562 kWh for heating.

C. Determination of electric load

The electrical consumption of the house modules consists of the utilization of 23 laptop workstations with their own lamps and ceiling lights (their consumption is about 9W and 23W, respectively, from technical specifications) projectors (with a consumed power of 190 W and they are supposed to work, at maximum load, four hours per day), ventilation and the heating system (i.e. the heat pump). In particular, the electrical demand is divided into a constant term during the day (the consumption related to ceiling lights) and a variable contribution, depending on the utilization of the nZEB. Moreover, some of the services provided to the users are common (heating and ventilation systems, ceiling lights and projectors), while the others are related to each individual workstation (electrical plugs for laptops connection and lamps). Representative loads profiles of laptops have been measured by a digital power meter with an uncertainty of ±0.3% of the full range for several months. Their consumed power is at peak ≈ 50W (a few minutes) during the start, then, at steady–state ≈ 30W.

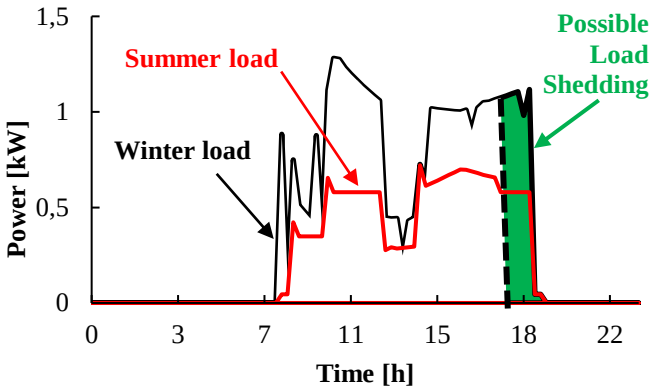

Fig. 8. Example of electrical load profile of a study room with heat pumps.

Fig. 8, presents the typical daily power profiles of one of the two identical study rooms, hosting 10 workstations. The load is higher during light-hours with a drop at lunchtime. During summer, the daily electrical consumption is 5.7 kWh/day and it includes cooling; the maximum power is ≈0.7 kW. During winter, the daily electrical consumption is 9.7 kWh/day including heating and the maximum load is ≈1.3 kW. Regarding electric seasonal demands, the study room requires 203 kWh/year for cooling and 217 kWh/year for heating. As described in Section II, load shedding could be adopted anticipating the closing hour of the building from ≈19:00 to ≈17:00, especially in winter months, when PV production is low. In this case study, if PV and storage installed on the study rooms cannot supply loads, the load is not interrupted. Thanks to the energy community, the load can be firstly supplied by the other users in the community, or by the external grid as a last chance.

Finally, the study room requires a heating demand of 894 kWh (Oct to Apr), while a cooling demand of 728 kWh (May to Sep). With respect to a traditional office building, which uses the heat pumps only for cooling purposes (heating load is supplied by fossil fuels), in the present nZEBs heat pumps satisfy also the heating demand, with a peak consumption in winter.

D. Design of optimal collection of solar energy

Regarding the inclination of the modules, the tilt coincides with the optimal value only in case of the control room, while the slopes of the PV generators on the other rooms are not optimal. In fact, tilts β and azimuths γ are purposely selected to simulate the installation of generators on the real four sloping sides of a hip roof. For control room, γ=26° and β=30°, while for technical room γ=-154° and β=10°. Units #2 and #3 have γ=-64° and β=20°, and γ=116° and β=20°, respectively. Finally, the selected slopes of the

roofs permit to minimize the effects of shadings on PV generators especially in winter, when the sun is low with the longest shadows, during central sunlight hours.

E. PV modelling and its experimental validation

The accurate assessment of PV production is fundamental to perform simulation of energy flows in microgrids, especially in cases in which production is totally based on PV technology. In the present subsection, a procedure is proposed to better estimate PV production by SDM. An accurate assessment of PV production is possible by using the single diode model. Nevertheless, as described in Section II, this model requires the use of the five parameters $\mu=[I_{ph}, I_0, n, R_{sh}, R_s]$ as inputs. These parameters are extracted from the measurement of the *I-V* curves of a m-Si PV module in several environmental conditions. The procedure has been performed as follows:

- *Measurements of I-V curves*: a commercial m-Si PV module, recently produced from one of the most important manufacturers at global level, was bought to be tested.

  It has a rated power of 300 W and efficiency of 18.3%. After the check of the absence of mechanical defects, performed by electroluminescence test [43], the electric tests were done. In particular, the *I-V* characteristic of the module was measured in several irradiance and temperature conditions, by using the capacitive method and the accurate instrumentation described in [44]. The measurement uncertainties are ±0.1 % for voltage and ±1 % for current. For the irradiance G, the uncertainty is of ±20 W/m^2, while for the ambient temperature T_a, the absolute uncertainty is of ±0.2 °C, and for the cell temperature T_C it is ±2°C. Finally, the absolute uncertainty for power is ±1%. Fig. 9 shows the measured *I-V* curves.
- *Parameters extraction*: the second step consists of the extraction of the five parameters from the *I-V* curves. Its aim is to find the optimal set of five parameters (used as inputs in the SDM) to trace a simulated *I-V* curve, which matches the best possible the measured curve of the PV generator. Different research works focus on finding efficient ways to extract the abovementioned parameters [45]. Two types of extraction methods have been developed, analytical [46] or evolutionary [47]. Analytical methods are faster and simpler, and equation (7) is solved in an explicit form, but they are strongly affected by the initial conditions. On the contrary, evolutionary techniques are more complex and require a bigger computational effort, but they do not depend on the initial parameters. In this work, the selected optimization technique is analytical and it uses the Lambert function. In particular, the Levemberg-Marquardt algorithm is used to minimize the Root Mean Square Error (RMSE) between experimental data and the I-V curve calculated with the single diode model [24].
- *Definition of the correlations for I_{ph} and I_0 with respect to temperature and irradiance variations*: in literature, the great majority of the works supposes a constant behaviour of the five parameters μ with respect to irradiance and temperature, or correlations based on few measurements. Nevertheless, it is an approximation limiting the accuracy of the production assessment [48]. In the present work, the measurements are performed on six irradiance levels in the range (≈140—880 W/m^2) and cell temperatures in the range (≈32—54 °C). The six sets of parameters are used in a fitting based on nonlinear correlations. Fig. 10 shows the evolution of I_0 with respect to cell temperature and the curve which fits the experimental points in an optimal way. The result of the procedure consists of two semi-empirical equations, describing the evolution of I_{ph} and I_0 as a function of temperature and irradiance. They can be used in equation (7) to calculate all the I-V characteristic in every environmental condition, with attention to the maximum power point.

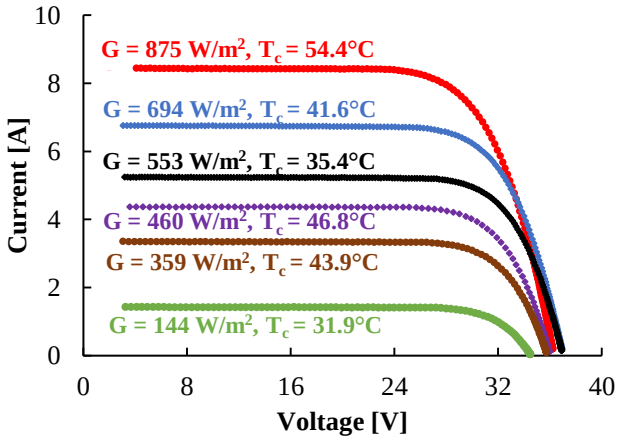

Fig. 9. Measured I-V curves at different G and T_c.

The effect of irradiance and cell temperature is different for the considered parameters: I_0 is only a function of the temperature (Fig. 10), while I_{ph} depends on both the variables (G,T_c), as shown in equation (14):

$$I_{ph}(G,T_c) = 9.45 \cdot \left[1 + \alpha_{I_{sc}} \cdot (T_c - T_{STC})\right] \cdot {}^{G}/_{G_{STC}} \quad (14)$$

Actually, the non-ideality factor, the series and parallel resistances are considered constant (n=1.25, R_s=0.39 Ω and R_{sh} = 211 Ω).

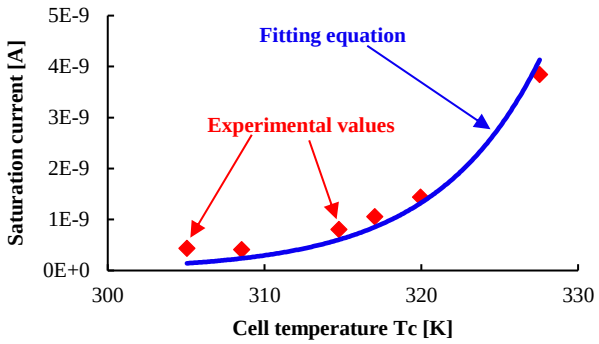

Fig. 10. Fitting of the saturation current values from the measurements.

Table II shows the results obtained using the above-reported semi-empirical correlations. They are compared with experimental results, as described in Section II. The first column contains irradiance levels, while the second one includes cell temperatures. The third column shows the measured maximum power P_{exp}, and P_{SDM} is the power calculated by the SDM.

TABLE II. POWER DEVIATIONS OF THE MODELS

G	T_c	P_{exp}	P_{SDM}	ΔP_{SDM}	
[W/m^2]	[°C]	[W]	[W]	[W]	[%]
875	54.4	223	223	0.3	0.1%
694	41.6	187	188	1	0.4%
553	35.4	149	154	5	4%
460	46.8	121	122	1	1%
359	43.9	93	96	3	3%
144	31.9	39	40	1	2%

The deviations of the model are evaluated with respect to the measured values $\Delta P_{SDM}=(P_{SDM}-P_{exp})$. In case of high irradiance (G>700 W/m^2), the SDM estimates the PV output with low deviations from measurements (ΔP_{SDM} ranges between 0.1% and 0.4%). In case of lower irradiances, the deviation ranges between 1% and 4%.

F. PV sizing

PV generation well matches the consumption of the nZEB for office/academic purposes, because higher loads occur during sunlight-hours. PV modules ensure good urban integration in terms of modularity (i.e. PV modules can be located according to the layout of the roof), fast installation and spaces exploitation. To maximize the space utilization, high-efficiency mono-crystalline (m-Si) modules [49] will be installed on the roof of the building, with a rated power of 360 W and an efficiency of 22.2%, provided at Standard Test Conditions (STC, with irradiance G_{STC}=1000 W/m^2, cell temperature T_{STC}=25°C and air mass AM=1.5) and *NOCT* equal to 45°C.

The size of the PV generators is defined according to the prescriptions in Section II, adapted for a microgrid with units sharing production and storage. Generally, the size of a PV generator is selected to supply the load of its single owner. In this case, they are sized to jointly produce an average winter daily production higher than the average load of all the units. Then, the single unit will exchange energy with the others, compensating surplus and deficit, as in a real energy community. As a result, the sum of the four generators sizes results 8.64 kW. The total PV capacity is divided in four plants with a size of 2.16 kW. In fact, following the logic of energy communities, the initial investment and related risk of investment are equally distributed between all the users. Adequate logics and tariffs will guarantee the cost effectiveness of exchanging energy inside the microgrid, with respect to the use of the grid. For example, to make energy exchange in the microgrid more convenient than actual net-billing scheme for domestic and tertiary-sector users in Italy [50], the surplus will be sold to other users at an intermediate tariff. Higher tariffs will be paid with respect to grid injection (≈13 c€/kWh), costs will be lower of energy paid for absorption from the grid (≈20 c€/kWh). In addition, a unique contract for grid connection reduces the overall fixed costs for the users.

G. Storage sizing

Regarding the storage, the criterion described in Section II is used, modified with the purpose of supporting the whole microgrid. In particular, all the storages have the overall capacity necessary to supply all the loads for more than a day, based on the analysis of the average consumption during the winter months. Capacities are equally distributed between users, following the logic of energy community, as done for PV. In case of small PV-storage applications, the lowest commercial battery capacity generally corresponds to $C_{E,batt}$=4 kWh. More battery units can be installed to increase the total capacity. Thus, if the minimum capacity is installed in each one of the four rooms, the total capacity is 16 kWh. As described in the previous section, control and technical rooms are part of the same unit with a capacity of 8 kWh. Each one of the two study rooms has a capacity of 4 kWh.

H. Power and energy simulation results for the microgrid

Fig. 11 shows the evolution of PV generation and electrical consumption for each nZEB during a typical winter day (15th January), when the incident irradiance on the PV generator is maximum (clear sky). As expected, the PV generation is the highest in the unit #1. Indeed, PV array has a well oriented string (SW), maximizing its production with a high daily power of about 1.5 kW. As a result, the daily PV production (7.4 kWh) is much higher than load (2.8 kWh). Thanks to storage, grid absorption is null, while the remaining surplus would be injected into the grid (4.4 kWh), if the energy community was not active. Thus, the self-sufficiency is 100%.

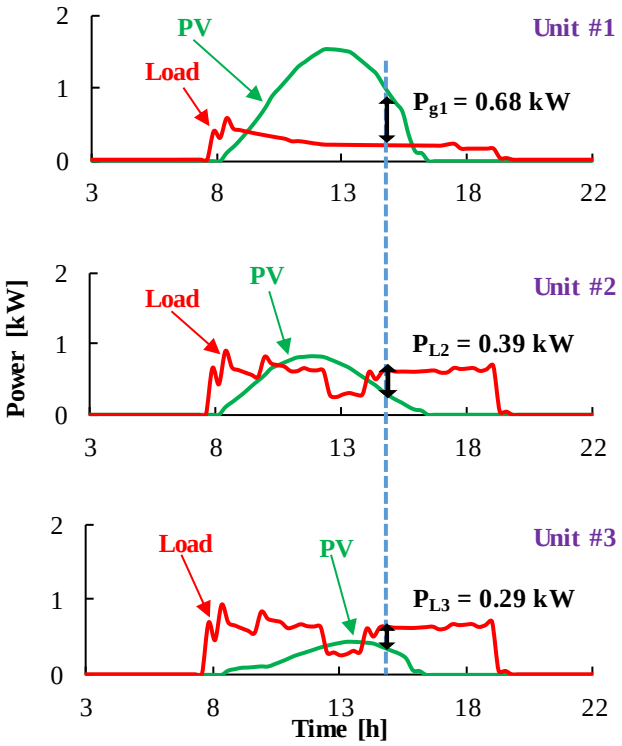

Fig. 11. Simulated PV and load profiles for the three units, 15th Jan.

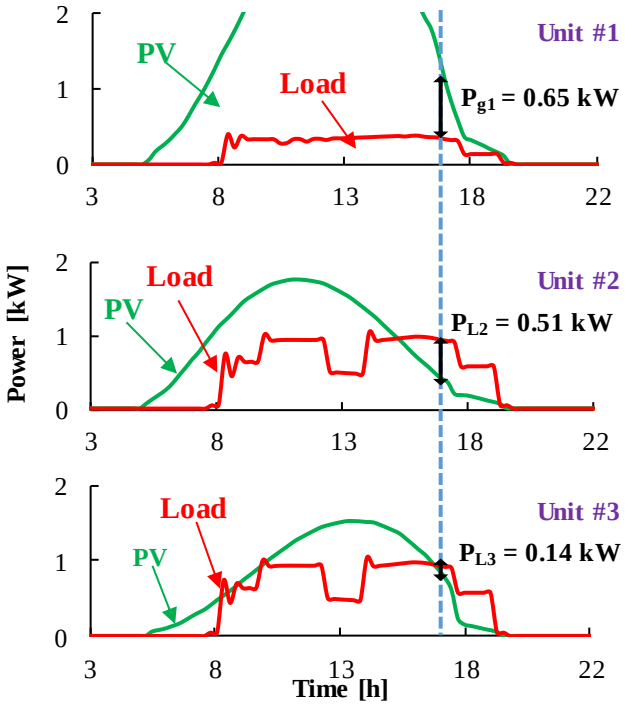

Fig. 12. Simulated PV and load profiles for the three units, 15th July.

On the contrary, the other two units are in energy deficit. In case of unit #2, the PV production is concentrated in the morning, because modules are SE oriented. Maximum power production occurs at midday (≈0.8 kW) and daily energy is 3.8 kWh, while load requires 6.5 kWh. During this day, the self-sufficiency is 59%. The worst case is unit #3: modules are NW oriented and the highest daily power is only 0.4 kW. The energy balance is the following: production is 2 kWh, consumption is 6.5 kWh, and absorption is 4.6 kWh. The self-sufficiency is low R_{ssuff}=30% and contribution of storage is negligible, because the low PV production is immediately used by loads. This case perfectly shows how an energy community can be useful in case of a poor matching between loads and generation of a single user. In particular, at 15:00, the PV and storage surplus in the control and technical rooms P_{g1} = 0.68 kW is shared with the other units. Loads of unit #2 and unit #3 are disconnected from their respective PV generators and connected to unit #1. As a consequence, the study rooms #1 and #2 absorb PL2 = 0.39 kW and PL3 = 0.29 kW, respectively, to improve the self-sufficiency of the whole microgrid.

Fig. 12 shows the profiles of PV production and the electrical demand for a typical summer day (15th July), with clear sky conditions. As a consequence of the sizing, performed to guarantee a high self-sufficiency during the whole year, the PV generation is much higher than load during summer. Unit #2 has a PV generation of 13.3 kWh and a consumption of 8.3 kWh, while unit#3 has a PV generation of 11.4 kWh and a consumption of 8.3 kWh. The highest generation occurs in control and technical rooms (25.1 kWh) with a peak of 4 kW (out of scale in the graph, to maintain the same axes), where the load is only 3.4 kWh. For all the units, the result is a daily R_{ssuff}=100%, thanks to batteries for supplying loads during evening. Nevertheless, the control and technical rooms would have a high grid injection (22 kWh) and a consequent low self-consumption (14%). Moreover, at 17:00, the surplus in unit #1 P_{g1} = 0.65 kW is shared with the other units, absorbing P_{L2} = 0.51 kW and P_{L3} = 0.14 kW.

In table III, the yearly energies are shown. In the first three columns, the energy flows and self-sufficiency of the single units are presented: they refer to a case without energy exchange between units. The last column contains the energy flows of all the units, exchanging energy as part of an energy community. Regarding the single units, the total self-sufficiency is reached by unit#1 (technical and control rooms), where PV generation is high, and load is low. In this configuration, no batteries are installed and the surplus is totally injected into the grid. This energy should be used by other units, when they are in deficit, especially during winter months. In particular, the unit#3 has the worst performance, with R_{ssuff}=47% and E_{abs}=858 kWh/year.

In Fig. 13 the yearly energy flows between the units in case of energy community is presented. Unit #1 provides the highest amount of surplus energy to the others (1752 kWh and 4014 kWh to unit #2 and unit #3, respectively). Moreover, unit #1 receives 2503 kWh from unit #2 while the other energy exchanges are negligible. The energy community permits a higher independence from the grid, with respect to the single users. In fact, the energy absorption decreases by ≈-37%, from 1800 to 1129 kWh/year. The grid injection varies from 6587 to 5915 kWh/year (corresponding to ≈-10%).On the contrary, the self-sufficiency increases from 54% to 71% (E_{glc} increases from 2072 to 2745 kWh/year).

TABLE III. YEARLY ENERGY RESULTS: SINGLE USERS VS. ENERGY COMMUNITY

	No energy exchange between units				Energy community
	Unit #1	**Unit #2**	**Unit #3**	**All**	**All**
E_{PV} [kWh]	4450	2361	1848	8659	8659
E_{load} [kWh]	622	1622	1628	3872	3872
E_{inj} [kWh]	3975	1534	1078	6587	5915
E_{abs} [kWh]	147	795	858	1800	1129
E_{glc} [kWh]	475	827	770	2072	2745
R_{ssuff}	76%	51%	47%	54%	71%

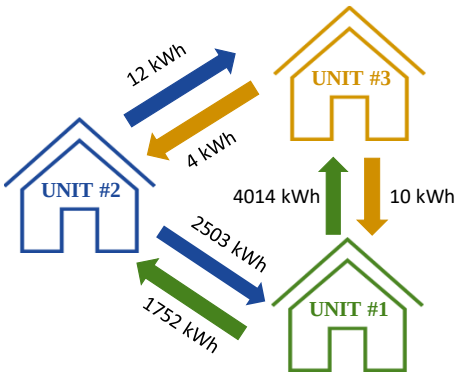

Fig. 13. Yearly energy flows between the units in case of no batteries installed.

Table IV shows an additional analysis regarding the evolution of the self-sufficiency R_{ssuff} obtained simulating different storage sizes, in case of both single users and energy community. In the simplest case, single users have no storage and do not exchange energy each other; their self-sufficiency is in the range 51—76%. On average, for all the buildings, R_{ssuff} is 54%, which is a typical

level for tertiary sector users supplied by PV generators. In the case study, the storage capacity $C_{E,batt}$=16 kWh increases the average self-sufficiency up to 74%. A negligible improvement could be obtained with $C_{E,batt}$= 32 kWh (R_{ssuff} increases from 74% to 77%). As expected, the last column in Table IV shows that the energy community increases the self-sufficiency in every case: without storage, R_{ssuff} increases from 54% to 71%, while R_{ssuff} is 100% with $C_{E,batt} \geq 16$ kWh.

TABLE IV. SELF-SUFFICIENCY WITH DIFFERENT STORAGE SIZES: SINGLE USERS VS. ENERGY COMMUNITY

		No energy exchange between units				**Energy community**
Overall storage capacity [kWh]		**Unit#1**	**Unit #2**	**Unit #3**	**All**	**All**
	0	76%	51%	47%	54%	71%
	16	100%	73%	65%	74%	100%
	32	100%	79%	68%	77%	100%

As a conclusion, the optimal configuration of the microgrid includes a storage capacity of 16 kWh because it permits to reach the complete independence from the electricity grid with the minimum storage capacity installed.

IV. CONCLUSIONS

This paper proposes a procedure to correctly design all-electric nZEBs, where heat pumps transform thermal demand in electric load, which is mainly supplied by local PV generators with storage. Both PV and batteries are simulated thanks to appropriate models, and the iterative procedure permits to define their sizes to guarantee an adequate level of self-sufficiency. Regarding the PV production assessment, the present work proposes an improved model, based on lumped parameters varying with irradiance and cell temperature. Results show that deviations between the proposed model and experimental data are always lower than 4% for all the irradiance levels. The whole design methodology is applied to a microgrid composed of three all-electric nZEBs, that share PV production and storage capacity to reach the highest possible grid-independence. The sizing procedure for PV and storage is applied at energy community level: all the plants in the different units are sized to satisfy the whole consumption in the microgrid, and not of the single users. The use of storage systems helps to compensate the local poor matching between load and production and the self-sufficiency raises from 54% without storage to 74%. Finally, the self-sufficiency is boosted up to 100% thanks to the energy community concept.

REFERENCES

[1] Directive 2010/31/EU of the European Parliament and of the Council, 19 May 2010.

[2] M. Medrano, J.M. Martí, L. Rincón, G. Mor, J. Cipriano, M. Farid, "Assessing the nearly zero-energy building gap in university campuses with a feature extraction methodology applied to a case study in Spain," *International Journal of Energy and Environmental Engineering*, pp.1-21, 2018.

[3] Jun Guan, Natasa Nord, Shuqin Chen, "Energy planning of university campus building complex: Energy usage and coincidental analysis of individual buildings with a case study" *Energy and Buildings*, Vol. 124, pp. 99-111, 2016.

[4] M. H. Chung, E. K. Rhee, "Potential opportunities for energy conservation in existing buildings on university campus: A field survey in Korea," *Energy and Buildings*, vol. 78, pp. 176-182, 2014.

[5] Umberto Berardi, Mauro Manca, Pau Casaldaliga, Felipe Pich-Aguilera, "From high-energy demands to nZEB: the retrofit of a school in Catalonia, Spain" *Energy Procedia*, Volume 140, pp. 141-150, 2017.

[6] Josh Wall, "Eco-Efficient Technology Solutions towards Net Zero: An Australian Case Study", *Energy Transformed Flagship CSIRO Energy Technology*, Australia, pp. 1-10, 2015.

[7] S. Hoque, "NET ZERO ENERGY HOMES: an evaluation of two homes in the northeastern United States," *J. Green Build*, pp. 79–90, 2010.

[8] L. Wells, B. Rismanchi, L. Aye, "A review of Net Zero Energy Buildings with reflections on the Australian context," *Energy and Buildings*, vol. 158, pp 616-628, 2018.

[9] G. Escrivá-Escrivá, "Basic actions to improve energy efficiency in commercial buildings in operation," *Energy and Buildings*, vol. 43, pp. 3106-3111, 2011.

[10] F. Spertino, G. Chicco, A. Ciocia, S. Corgnati, P. Di Leo and D. Raimondo, "Electricity consumption assessment and PV system integration in grid-connected office buildings," in *Proc. 2015 IEEE 15th International Conference on Environment and Electrical Engineering (EEEIC)*, pp. 255-260.

[11] F. Spertino, J. Ahmad, G. Chicco, A. Ciocia and P. Di Leo, "Matching between electric generation and load: Hybrid PV-wind system and tertiary-sector users," in *Proc. 2015 50th International Universities Power Engineering Conference (UPEC)*, pp. 1-6.

[12] UNI EN ISO 13790:2008. Energy performance of buildings. Calculation of energy use for space heating and cooling. Dec 2008.

[13] UNI 10339:1995 "Impianti aeraulici al fini di benessere. Generalità, classificazione e requisiti. Regole per la richiesta d'offerta, l'offerta, l'ordine e la fornitura", CTI, 1995, in Italian language.

[14] S. Klyapovskiy, S. You, H. Cai and H. W. Bindner, "Integrated Planning of a Large-Scale Heat Pump in View of Heat and Power Networks," *IEEE Transactions on Industry Applications*, vol. 55, no. 1, pp. 5-15, Jan.-Feb. 2019.

[15] A.C. Gillet, "Heat pumps and renewable energies," *Renewable Energy*, Volume 9, Issues 1–4, Pages 641-644, 1996.

[16] Octávio Alves, Eliseu Monteiro, Paulo Brito, Pedro Romano, "Measurement and classification of energy efficiency in HVAC systems," *Energy and Buildings*, Volume 130, Pages 408-419, 2016.

[17] H. Pieper, T. Ommen, W. Markussen, B. Elmegaard, "Optimal usage of low temperature heat sources to supply district heating by heat pumps," in *Proc. 30th Int. Conf. Efficiency Cost Optim. Simul. Environ. Impact Energy Syst*., pp. 1-16, 2017.

[18] D. A. Brodén, K. Paridari and L. Nordström, "Matlab applications to generate synthetic electricity load profiles of office buildings and detached houses," *IEEE Innovative Smart Grid Technologies - Asia (ISGT-Asia)*, Auckland, pp. 1-6, 2017.

[19] L. Chuan, D. M. K. K. V. Rao and A. Ukil, "Load profiling of Singapore buildings for peak shaving," in *Proc. 2014 IEEE PES Asia-Pacific Power and Energy Engineering Conference (APPEEC)*, pp. 1-6.

[20] European Commission, Joint Research Centre, Institute for Energy and Transport, "Photovoltaic Geographical Information System (PVGIS)", available at http://re.jrc.ec.europa.eu/pvgis/.
[21] N. Barth, R. Jovanovic, S. Ahzi, M. A. Khaleel, "PV panel single and double diode models: Optimization of the parameters and temperature dependence," *Solar Energy Materials and Solar Cells*, vol. 148, pp. 87-98, 2016.
[22] M. Muller, B. Marion, J. Rodriguez, "Evaluating the IEC 61215 Ed.3 NMOT procedure against the existing NOCT procedure with PV modules in a side-by-side configuration," in *Proc. 2012 38th IEEE Photovoltaic Specialists Conference*, pp. 697-702.
[23] Mohamed B.H. Rhouma, Adel Gastli, Lazhar Ben Brahim, Farid Touati, Mohieddine Benammar, "A simple method for extracting the parameters of the PV cell single-diode model," *Renewable Energy*, Volume 113, pp. 885-894, 2017.
[24] Xiankun Gao, Yan Cui, Jianjun Hu, Guangyin Xu, Zhenfeng Wang, Jianhua Qu, Heng Wang, "Parameter extraction of solar cell models using improved shuffled complex evolution algorithm," *Energy Conversion and Management*, Volume 157, pp. 460-479, 2018.
[25] E. Gadjeva and G. Kunov, "Application of postprocessing in probe for automated model parameter extraction of photovoltaic panels," *IEEE 23rd International Symposium for Design and Technology in Electronic Packaging (SIITME)*, Constanta, pp. 227-230, 2017.
[26] Ortiz-Conde, Adelmo & García-Sánchez, Francisco & Muci, Juan & Sucre-González, Andrea. "A review of diode and solar cell equivalent circuit model lumped parameter extraction procedures" *Facta Universitatis, Series: Electronics and Energetics*, 2014.
[27] F. Spertino, A. Ciocia, P. Di Leo, R. Tommasini, I. Berardone, M. Corrado, A. Infuso, M. Paggi, "A power and energy procedure in operating photovoltaic systems to quantify the losses according to the causes," *Solar Energy*, vol. 118, pp. 313-336, 2015.
[28] A. Ciocia, J. Ahmad, G. Chicco, P. Di Leo and F. Spertino, "Optimal size of photovoltaic systems with storage for office and residential loads in the Italian net-billing scheme," in *Proc. 2016 51st International Universities Power Engineering Conference (UPEC)*, Coimbra, pp. 1-6.
[29] F. Giordano, A. Ciocia, P. Di Leo, F. Spertino, A. Tenconi and S. Vaschetto, "Self-Consumption Improvement for a Nanogrid with Photovoltaic and Vehicle-to-Home Technologies," in *Proc. 2018 IEEE International Conference on Environment and Electrical Engineering and 2018 IEEE Industrial and Commercial Power Systems Europe (EEEIC / I&CPS Europe)*, Palermo, pp. 1-6.
[30] A. A. Hussein and I. Batarseh, "An overview of generic battery models," in *Proc. 2011 IEEE Power and Energy Society General Meeting*, pp. 1-6.
[31] Min Chen and G. A. Rincon-Mora, "Accurate electrical battery model capable of predicting runtime and I-V performance," in *IEEE Transactions on Energy Conversion*, vol. 21, no. 2, pp. 504-511, June 2006.
[32] T. Xia, M. Li, P. Zi, L. Tian, X. Qin., N. An, "Modeling and simulation of Battery Energy Storage System (BESS) used in power system," in *Proc. 2015 5th International Conference on Electric Utility Deregulation and Restructuring and Power Technologies* (DRPT), pp. 2120-2125.
[33] M. B. Téllez. Molina, M. Prodanovic, "Profitability assessment for self-sufficiency improvement in grid-connected non-residential buildings with on-site PV installations," in *Proc. 2013 International Conference on Clean Electrical Power (ICCEP)*, pp. 353-360.
[34] International Energy Agency, "Review and Analysis of PV Self-consumption Policies", 2019.
[35] G. Tsagarakis, R. C. Thomson, A. J. Collin, G. P. Harrison, A. E. Kiprakis and S. McLaughlin, "Assessment of the Cost and Environmental Impact of Residential Demand-Side Management," in *IEEE Transactions on Industry Applications*, vol. 52, no. 3, pp. 2486-2495, May-June 2016.
[36] L. Martirano et al., "Demand Side Management in Microgrids for Load Control in Nearly Zero Energy Buildings," in *IEEE Transactions on Industry Applications*, vol. 53, no. 3, pp. 1769-1779, May-June 2017.
[37] Komatsu, K., Mori, T., Kitamori, A., Araki, Y. "Evaluation on dynamic performance of glulam frame structure composed of slotted bolted connection system" in *Proc*. 2014 *World Conference on Timber Engineering.*
[38] J. Ahmad, F. Spertino, P. Di Leo and A. Ciocia, "A Variable Step Size Perturb and Observe Method Based MPPT for Partially Shaded Photovoltaic Arrays," in *Proc. PCIM Europe 2016; International Exhibition and Conference for Power Electronics, Intelligent Motion, Renewable Energy and Energy Management*, pp. 1-8.
[39] J. Ahmad, F. Spertino, P. Di Leo and A. Ciocia, "An efficient maximum power point tracking algorithm for photovoltaic arrays under partial shading conditions," in *Proc. 2016 IEEE International Power Electronics and Motion Control Conference (PEMC*, pp. 322-327.
[40] M. Beccali, G. Ciulla, V. Lo Brano, A. Galatioto, M. Bonomolo, "Artificial neural network decision support tool for assessment of the energy performance and the refurbishment actions for the non-residential building stock in Southern Italy," *Energy*, vol. 137, pp. 1201-1218, 2017.
[41] D.M. 26/06/2015. Linee guida nazionali per la certificazione energetica degli edifici. June 2015.
[42] Passive House Institute, "Passive House requirements," Online: www.passiv.de/en/02_informations/02_passive-house-requirements/02_passive-house-requirements.htm.
[43] B. B. Yang, J. L. Cruz-Campa, G. S. Haase, E.I. Cole, P. Tangyunyong, P. J. Resnick, A. C. Kilgo, M. Okandan, G. N. Nielson, "Failure Analysis Techniques for Microsystems-Enabled Photovoltaics," *IEEE Journal of Photovoltaics*, vol. 4, no. 1, pp. 470-476, Jan. 2014.
[44] F. Spertino, J. Ahmad, A. Ciocia, P. Di Leo, A. F. Murtaza, M. Chiaberge, "Capacitor charging method for I–V curve tracer and MPPT in photovoltaic systems," *Solar Energy*, vol. 119, pp. 461-473, 2015.
[45] A. Gastli, L. Ben-Brahim, M. B. H. Rhouma, "ANN-based extraction approach of PV cell equivalent circuit parameters," in *Proc. 2015 17th European Conference on Power Electronics and Applications* (EPE'15 ECCE-Europe), pp. 1-10.
[46] D. S. H. Chan, J. C. H. Phang, "Analytical methods for the extraction of solar-cell single- and double-diode model parameters from I-V characteristics," *IEEE Transactions on Electron Devices*, vol. 34, no. 2, pp. 286-293, 1987.
[47] Z. M. Omer, A. A. Fardoun, A. Hussain, "Large scale photovoltaic array fault diagnosis for optimized solar cell parameters extracted by heuristic evolutionary algorithm," in *Proc. 2016 IEEE Power and Energy Society General Meeting* (PESGM), Boston, pp. 1-5.
[48] A. Harrag, S. Messalti, "Three, Five and Seven PV Model Parameters Extraction using PSO," *Energy Procedia*, vol. 119, pp. 767-774, 2017.
[49] M. Gürtürk, H. Benli, N. K. Ertürk, "Effects of different parameters on energy – Exergy and power conversion efficiency of PV modules," *Renewable and Sustainable Energy Reviews*, vol. 92, pp. 426-439, 2018.
[50] Gestore Servizi Energetici (GSE), Solare Fotovoltaico – "Rapporto Statistico2017", available online https://www.gse.it